

Effect of reduced local lattice disorder on the magnetic properties of B-site substituted $\text{La}_{0.8}\text{Sr}_{0.2}\text{MnO}_3$

Sagar Ghorai^{1*}, Sergey A. Ivanov^{1,2}, Ridha Skini¹, Petter Ström³ and Peter Svedlindh¹

¹ Department of Materials Science and Engineering, Uppsala University, Box 35, SE-751 03, Uppsala, Sweden

² Semenov Institute of Chemical Physics, Kosygin Street, 4, Moscow, Russia, 119991

³ Applied Nuclear Physics, Department of Physics and Astronomy, Uppsala University, Box 516, SE-751 20 Uppsala, Sweden

ABSTRACT

Disorder induced by chemical inhomogeneity and Jahn-Teller (JT) distortions is often observed in mixed valence perovskite manganites. The main reasons for the evolution of this disorder are connected with the cationic size differences and the ratio between JT active and non-JT active ions. The quenched disorder leads to a spin-cluster state above the magnetic transition temperature. The effect of Cu, a B-site substitution in the $\text{La}_{0.8}\text{Sr}_{0.2}\text{MnO}_3$ compound, on the disordered phase has been addressed here. X-ray powder diffraction reveals rhombohedral (R-3c) structures for the two compounds with negligible change of lattice volume. The chemical compositions of the two compounds were verified by ion beam analysis technique. With the change of electronic bandwidth, the magnetic phase transition temperature has been tuned towards room temperature (318 K), an important requirement for room temperature magnetic refrigeration. However, a small decrease of the isothermal entropy was observed with Cu-substitution, related to the decrease of the saturation magnetization.

*Correspondence to: sagar.ghorai@angstrom.uu.se

Mixed valence perovskite manganite oxides ($\text{A}_x\text{B}_{1-x}\text{MnO}_3$) have attained much attention owing to magnetic disorder driven by competing magnetic interactions and coupling between charge, spin, lattice and orbital degrees of freedom.¹ Mostly, they exhibit two types of exchange interactions; ferromagnetic (FM) double-exchange interaction via $\text{Mn}^{3+}\text{-O}^{2-}\text{-Mn}^{4+}$ and antiferromagnetic (AFM) superexchange interaction via $\text{Mn}^{3+}\text{-O}^{2-}\text{-Mn}^{3+}$ (or $\text{Mn}^{4+}\text{-O}^{2-}\text{-Mn}^{4+}$). Depending on the $\text{Mn}^{3+}/\text{Mn}^{4+}$ ratio there will be a varying degree of competing FM-AFM interactions. The competing interactions can cause magnetic disorder in manganites, which is often revealed by a Griffiths phase (GP) singularity.² In the original work of Griffiths,³ a randomly diluted Ising ferromagnetic system was considered with only a fraction of the lattice-sites occupied with nearest-neighbour interacting Ising spins. If the lattice system is considered as a state ψ , and lattice-sites with and without Ising spins are described as $v(\psi)$ and $s(\psi)$, respectively, then the probability of the lattice system can be written as,

$$P(\psi) = P(v) + P(s) = 1.$$

For an undiluted or homogeneous ferromagnetic system, $P(s) = 0$.²⁻⁴ For $P(v) < 1$, above a certain value (percolation threshold), long-range ferromagnetic order is complete at a probabilistic transition temperature $T_C(P(v))$, which is less than the transition temperature of an undiluted system.³ In case of $P(v) < 1$, ferromagnetic order begins to develop below the Griffiths temperature (T_G) as finite size ferromagnetically ordered spin-clusters. The temperature region between T_G and T_C is defined as the GP-region.⁴ Obviously, the width of the GP-region depends on $P(v)$, but in systems with competing FM and AFM interactions it will also depend on the relative amount and strength of these interactions. Thus, in perovskite manganites with competing exchange interactions, the $\text{Mn}^{3+}/\text{Mn}^{4+}$ ratio can tune the width of the GP-region.

Previously, the evolution of the GP-region in manganites has been studied for different A-site substitutions.⁵⁻¹² However, in most cases A-site substitution introduces a change of lattice volume or even a change in crystal structure, which does not concur with the original model of Griffiths.³ Thus, A-site substitution often introduces additional changes in the system that can mask the effect of disorder on the evolution of the GP phase.

There are only a few reports,^{2,13} which describe the dependence of the GP phase on B-site substitution and the reason for an increasing or decreasing width of the GP region in B-site substituted manganites is not clear. The strength and the relative amount of FM and AFM interactions between B-site atoms will act together with local lattice distortions due to Jahn-Teller active ions govern the formation and evolution of ferromagnetic clusters above T_C .

In this work we have substituted the B-site of $\text{La}_{0.8}\text{Sr}_{0.2}\text{MnO}_3$ with magnetic Cu-atoms. With the support of electronic structure analysis, we have characterized the magnetic interactions between B-site atoms and their effect on the formation of the GP phase. As manganites can be tuned to act as a magnetic refrigerant near room temperature,¹⁴ the effect of B-site substitution on the magnetocaloric effect has also been studied in this work. A comparatively high value of isothermal entropy change (see **Table 1**) over a wide temperature span, makes this substitution interesting for room temperature magnetic refrigeration applications.

The $\text{La}_{0.8}\text{Sr}_{0.2}\text{MnO}_3$ (**LS**) and $\text{La}_{0.8}\text{Sr}_{0.2}\text{Mn}_{0.9}\text{Cu}_{0.1}\text{O}_3$ (**LSC**) compounds were prepared by solid-state reaction. Stoichiometric amounts of La_2O_3 , Sr_2O_3 , MnCO_3 and CuO powders were mixed together and calcinated at 1473 K for 24 h in Ar-atmosphere. The samples were characterized using X-ray powder diffraction (XRPD) at 295 K by using a Bruker D8 Advance diffractometer with $\text{Cu}-\text{K}\beta$ radiation and an angle step size of 0.013° (15 s per step). The elemental analysis of the samples was performed by time-of-flight elastic recoil detection analysis (ToF-ERDA)¹⁵ with 36 MeV $^{127}\text{I}^{8+}$. The incidence angle of the ion-beam was $23^\circ \pm 1^\circ$ with respect to the sample surface, and recoils were detected at 45° . Simultaneous Rutherford backscattering spectrometry (RBS) and particle induced X-ray emission (PIXE) with a 2 MeV $^4\text{He}^+$ beam and detectors at 170° (RBS) and 135° (PIXE) were also applied. X-ray photoelectron spectroscopy (XPS) was used to analyse the oxidation states and valence band spectra of the samples. The XPS spectra were collected by using a "PHI Quantera II" system with an $\text{Al}-\text{K}\alpha$ X-ray source and a hemispherical electron energy analyser having a pass energy of 26.00 eV. Pre-sputtering with Ar-ions of 200 eV for 30 seconds was done on the samples before collecting the XPS spectra in order to remove surface impurities without affecting the sample's

properties. A Quantum Design MPMS XL system was used to measure the magnetic properties in the temperature range from 390 K to 5 K with a maximum field of 5 T.

The analysis of the XRPD spectra (**Figure 1(a)** and (**b**)) with Fullprof program¹⁶ reveals a single phase rhombohedral structure for the two compounds. During XRPD analysis several structural models, orthorhombic, monoclinic, rhombohedral, etc. were fitted and the best fit of the structural model was observed for the rhombohedral structure with a space group R-3c. The structural parameters are listed in **Table 1**. The absence extra peaks and similar lattice parameters in the Cu-substituted compound, confirm that the Cu-atoms have substituted the Mn-site (6e-site) of the lattice.

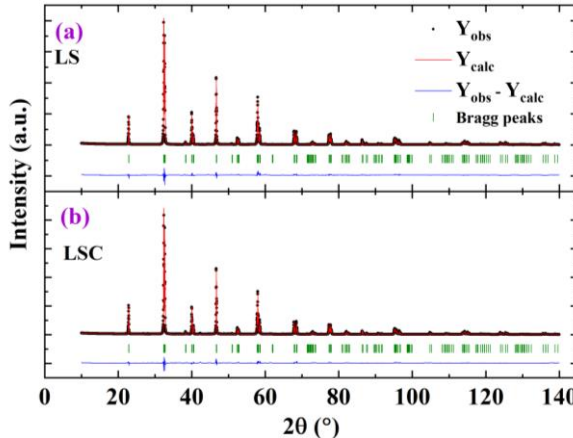


Figure 1: X-Ray powder diffraction patterns of (a) LS and (b) LSC samples.

The crystal structure can also be described with the Goldschmidt tolerance factor¹⁷ ($t_G = \frac{r_A + r_O}{\sqrt{2}(r_B + r_O)}$, where r_A , r_B and r_O are the ionic radii of A, B and oxygen ions, respectively). For the LS and LSC compounds the values of t_G are very close (0.921 and 0.923, respectively) even if the mixed valence of Cu (+2 and +3 oxidation states) is considered (from XPS analysis, described later). The t_G values are calculated using the ionic radius (calculated by R. D. Shannon¹⁸) of the La⁺³, Sr²⁺, Mn³⁺, Mn⁴⁺, Cu²⁺, Cu³⁺ and O⁻² ions as 1.216, 1.31, 0.645, 0.53, 0.73, 0.54 and 1.4 Å, respectively. This minimal difference in the crystal structures of the two compounds provides the opportunity to study the effect of disorder and GP-evolution without influence from a crystal structure change as mentioned in the introduction.

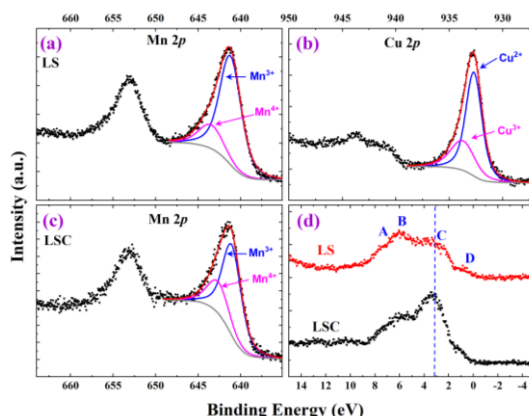


Figure 2: XPS spectra of (a) Mn 2p state of LS compound, (b) Cu 2p state of the LSC-compound, (c) Mn 2p state of LSC-compound and (d) valence band spectra of LS and LSC compounds.

Two oxidation states for both Mn (+3 and +4) and Cu (+2 and +3) are observed from the XPS Mn 2p (**Figure 2(a)** and (**c**)) and Cu 2p (**Figure 2(b)**) core level spectra.^{20,21} From the analysis of the $2p_{3/2}$ peaks of Mn and Cu the relative amounts of the different oxidation states have been calculated and are listed in **Table 1**.

The calculated values are comparable to the expected values for both the compounds. The chemical formula for the LS and LSC compounds can be written as,

$La^{+3}Sr^{+2}Mn_x^{+3}Mn_{(1-p-x)}^{+4}Cu_y^{+2}Cu_{(p-y)}^{+3}O_{3+z}^{-2}$, where x , y and z correspond to the amount of Mn³⁺, Cu²⁺ and extra O⁻² ions, respectively, and p to the total amount of Cu ions. From charge neutrality we have,

$$x + y + p + 2z = 0.8. \quad (1)$$

Here, p is 0 and 0.1 for the LS and LSC compounds, respectively. Thus, using the value of x from **Table 1**, for the LS compound the value of z becomes -0.0005 . Similar small negative value of z (-0.0066) is obtained for the LSC compound by considering the values of x and y from **Table 1**. Considering the error in the XPS results, we have to keep in mind that the above-mentioned values are only approximate estimates, made to justify the negligible O-deficiency in both of the compounds.

Table 1 Structural, electronic, chemical and magnetic results

Compound	LS	LSC	
Space Group	R-3c	R-3c	
Lattice parameters (Å)	<td>$a = 5.52240(4)$</td> <td>$a = 5.52280(4)$</td>	$a = 5.52240(4)$	$a = 5.52280(4)$
	<td>$c = 13.33689(12)$</td> <td>$c = 13.3630(11)$</td>	$c = 13.33689(12)$	$c = 13.3630(11)$
Mn-O Bond lengths (Å)	1.9642(7)	1.9664(7)	
Mn-O-Mn Bond angle (°)	163.90(16)	162.99(17)	
Rietveld Refinement Parameters ¹⁹ for XRPD	R_P 7.32 R_{WP} 9.77 R_B 5.27	6.19 8.31 4.90	
Mn ³⁺ /Mn ⁴⁺	80.1(14)/ 19.9(14)	71.5(11)/ 28.5(11)	
Cu ²⁺ /Cu ³⁺	-	69.8(10)/ 30.2(10)	
Atomic % from TOF-ERDA	Mn 22.2(12) Cu - O 59.3(33)	20.6(11) 2.0(2) 58.3(31)	
T_c (K)	330(2)	318(2)	
M_s (Am ² /kg)	90.99	81.40	
$-\Delta S_M^{max}$ (J/kg-K) at 5T	5.18	4.53	
RCP (J/kg) at 5T	245	230	

The magnetic properties of the LS and LSC compounds are strongly dependent on the amount of Mn and Cu mixed valence. Moreover, the oxidation states of the B-site ions are also dependent on the amount of oxygen present in the compounds. From the XPS analysis we know that the O-deficiency is negligible in the two compounds, which gives the opportunity to directly analyse the influence of the B-site substitution on the magnetic properties.

The valence band spectra for LS and LSC compounds are shown in **Figure 2(d)**. In general, the valence band spectrum of a perovskite manganite has four binding energy contributions A, B, C and D, as indicated in **Figure 2(d)**, where A corresponds to the O^{2p}-Mn^{3d} t_{2g} hybridized state, B to the nonbonding O^{2p} state, C to the Mn^{3d} t_{2g} state and D to the Mn^{3d} e_g state.²²⁻²⁴ In the LSC compound there is a contribution from the Cu^{3d} orbital in the binding energy range 2-4 eV,²⁰ which is revealed by the increase of density of states for these energies. Also, from theoretical calculations it is known that only the e_g state of Cu^{3d} will contribute to the density of states below the Fermi-level,²⁰ which is an indication of the strong coupling between the Mn^{3d} t_{2g} and Cu^{3d} e_g orbitals and the nature of this coupling (FM or AFM) will decide the magnetic properties of the LSC compound.

Raw ToF-ERDA data is shown in **Figure 3(a) and (b)**. In addition to the expected elemental contents, impurity signals due to approximately 0.5-1.5 at. % of H and C were detected on both samples. For the LSC sample, a faint signal due to Si or Al contamination was detected, part of which may be attributed to the beam grazing the Al sample holder. Depth profiling of the ToF-ERDA data with Potku²⁵, including all detected signals, and integration from depth 1.5×10^{17} at/cm² to 1.5×10^{18} at/cm² yielded an estimation of the sample composition. The obtained RBS data indicated concentration gradients for La and Sr near the sample surface, making fitting of the relative concentrations ambiguous. Further, a heavy impurity at concentration $\lesssim 0.2$ at. % was detected, identified as Pb from the PIXE spectra shown in **Figure 3(c)**.

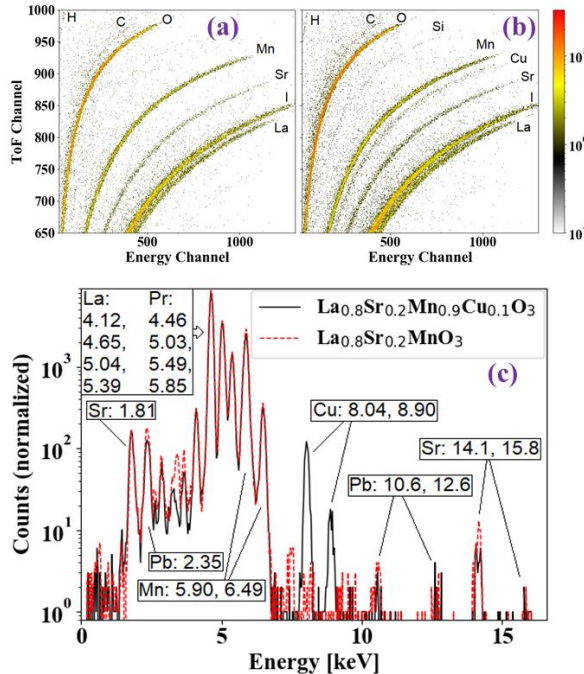


Figure 3: Raw ToF-ERDA data for samples (a) LS and (b) LSC. (c)PIXE spectra obtained on LS and LSC samples, with detected elements indicated. The peaks observed between the Pb Ma-line at 2.35 keV and the set of L-lines from La and Pb are a combination of other Pb M-lines and escape peaks due to excitations in the Si drift detector.

For Mn, the number of counts in the region of the ToF-ERDA spectrum from which data was considered is between approximately 1000 and 2500 for the two samples, yielding a relative statistical uncertainty of 2-3%. The corresponding number for Sr and Cu is 4-5%, while background counts amount to approximately 5-8% of the collected data from these elements. Further, an uncertainty in relative detection efficiency between Mn or Cu and O contributes an error up to 5%. The atomic fractions of Mn, O and Cu obtained from ToF-ERDA are listed in **Table 1** and they are comparable with the expected values. Varying the integration depth over a range up to a maximum of 2×10^{18} at/cm², to ascertain the effect of near-surface concentration gradients, yields a variation of the Mn, O and Cu concentrations within the given error margins.

A second order paramagnetic to ferromagnetic (PM-FM) transition was observed (using Banerjee Criterion²⁶⁻²⁹) in both compounds. However, the transition temperature (T_C) decreased with Cu-substitution (from 330K to 318K, cf. **Figure 4(a)**). Since double-exchange interaction is responsible for the ferromagnetism in the two compounds, one expects that T_C should be governed by the electronic bandwidth (W),³⁰ which is defined as,

$$W \propto \frac{\cos(1/2(\pi - (Mn - O - Mn)))}{d_{Mn-O}^{3.5}}, \quad (2)$$

where $\langle Mn - O - Mn \rangle$ and d_{Mn-O} are the bond angle and bond length, respectively. From **Table 1**, a decrease of W is observed with Cu-substitution, which is in accord with the observed decrease of T_C , and in good agreement with previously reported results on manganites.³⁰ Moreover, Cu-substitution introduces a new AFM Mn^{3+} - O^{2-} - Cu^{2+} superexchange interaction³¹ in the compound and also reduces the saturation magnetization (cf. **Figure 4(b)**).

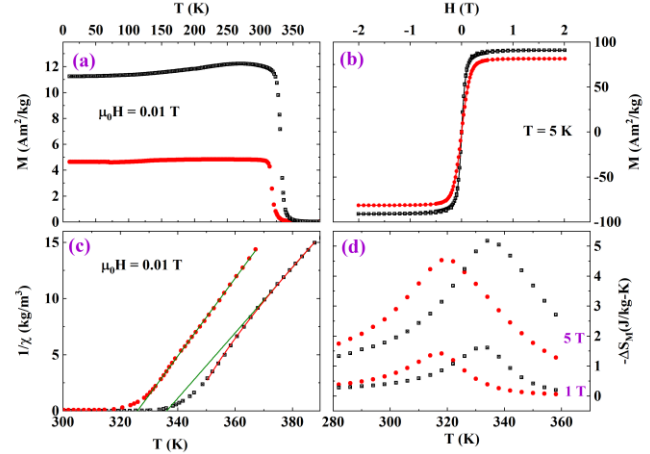


Figure 4: (a) Low-field magnetization versus temperature and (b) magnetization versus magnetic field at 5 K. Temperature dependence of (c) inverse susceptibility and (d) isothermal entropy change for LS and LSC samples. Black (red) data-points give the result for LS (LSC) compound.

A Griffiths phase like behaviour was observed in the LS compound (**Figure 4(c)**), implying that ferromagnetically ordered clusters are formed in the paramagnetic region below the Griffiths temperature T_G . The GP, which is suppressed in the LSC compound, can be characterized by the temperature dependence of the magnetic susceptibility according to²

$$\chi^{-1} \propto (T - T_C^R)^{1-\lambda}, \quad (3)$$

where $0 \leq \lambda < 1$ and T_C^R is the critical temperature where the susceptibility tends to diverge. The different transition temperatures T_C , T_G , T_C^R are determined following the method discussed by A.K. Pramanik *et al.*² In **Figure 4(c)**, the red line indicates the fitting of the inverse susceptibility of the LS compound below T_G with **Equation (3)**. The temperature range of the GP is described as,²

$$GP\% = \frac{T_G - T_C}{T_C} \times 100. \quad (4)$$

Both λ and GP% decrease with increasing magnetic field; λ (GP%) was found to be 0.29, 0.24 and 0.12 (15%, 13% and 12%) for applied fields of 0.01mT, 0.5mT and 0.1mT, respectively in the LS compound. This indicates that the GP will vanish above a certain threshold magnetic field.

In the $La_{(1-x)}Sr_xMnO_3$ system, Jahn-Teller (JT) distortions have been identified as the reason for the appearance of the GP.⁸ JT distortions exist for Mn^{3+} ions, as there is only one electron in a degenerate e_g -state and to reduce its energy there will be a geometrical distortion along one of the fourfold axes. For the Mn^{4+} ion there is no JT distortion since no electron occupies the e_g -state. Similarly, Cu^{2+} ions exhibit a JT distortion, while Cu^{3+} ions don't. From the balance of valence charges, Cu^{2+} substitution will increase the amount of Mn^{4+} ions and decrease the amount of Mn^{3+} ions. The substitution is straight forward for Cu^{3+} , it only replaces Mn^{3+} ions. As a combined effect of Cu^{2+} and Cu^{3+} substitutions, the ratio of JT ions (Mn^{3+} and Cu^{2+}) to non-JT ions (Mn^{4+} and Cu^{3+}) will decrease. A direct evidence of this argument is observed in the XPS analysis, with Cu-substitution the ratio of JT/non-JT ions decreased from 4.02 to 2.49.

Two types of JT distortions have been identified; pairs of weakly distorted Mn^{3+} - Mn^{4+} ions, each pair sharing an electron-hole pair, and isolated Mn^{3+} ions exhibiting considerably larger

lattice distortions.³² The energy barrier for activated hopping of charge carriers will be large for isolated Mn^{+3} ions, while the barrier will be much reduced for pairs of Mn^{+3} - Mn^{+4} ions, referred to as dimers by Kumar *et al.*³³ and dimerons by Downward *et al.*³⁴ Dimerons form at some temperature above T_c (here related to T_G), where there is a deviation from the Curie-Weiss law in the temperature dependent susceptibility plot, and favour ferromagnetic double-exchange interaction via mobile charge carriers. As the magnetic transition temperature is approached, dimerons will form small clusters and the development of these clusters is similar to diffusion limited aggregation.³⁴ The formation of spin clusters depends on the amount of local lattice distortions and the availability of electron hole-pairs in the compound. The overall decrease of JT-active ions in the Cu substituted restricts the formation of spin clusters, implying that the compound from a magnetic perspective becomes more homogeneous.

The magnetocaloric (MCE) properties have been characterized in terms of the isothermal entropy change using magnetometry. From Maxwell's relation the isothermal entropy change (ΔS_M) can be expressed as,¹⁴

$$\Delta S_M = \mu_0 \int_{H_i}^{H_f} \left(\frac{\partial M}{\partial T} \right)_H dH, \quad (5)$$

where μ_0 is the free-space permeability, H_i and H_f are the initial and final applied magnetic fields, respectively. Also, for real applications it is important to realise a sufficiently large effective temperature range in which a refrigeration process will work and the relative cooling power (RCP)¹⁴ is a measure of this. The RCP is defined as,

$$RCP = -\Delta S_M^{max} \times \Delta T_{FWHM}, \quad (6)$$

where $-\Delta S_M^{max}$ is the isothermal entropy change maximum and ΔT_{FWHM} is the full width at half maximum of the $-\Delta S_M$ versus temperature curve. The field and temperature dependence of the isothermal entropy change for the LS and LSC compounds are shown in **Figure 4(d)**. The maximum value of isothermal entropy change was observed near T_c for both compounds. At an applied field of 5T, the entropy maximum and the RCP value decrease by 12.5% and 6%, respectively with 10% Cu-substitution in the B-site. This is also expected from the decrease of the saturation magnetization with Cu-substitution. However, Cu-substitution is still of value as it lowered the temperature where ΔS_M^{max} occurs towards room temperature.

The effect of partial substitution of Mn with Cu in $La_{0.8}Sr_{0.2}MnO_3$ on structural, electronic, chemical, magnetic and magnetocaloric properties are described here. Rhombohedral (R-3c) structures with almost the same lattice parameters were observed for the two compounds, which allows for a purer investigation of how lattice distortion and competing magnetic interactions (arising from additional AFM interactions of type Mn^{+3} - O^{2-} - Cu^{+2}) affect the evolution of a GP. From XPS analysis negligible amount of O-deficiency was observed for the two compounds, which is also important to avoid effect of anions on the valence charge of B-site magnetic ions. In the LS compound, the GP was observed due to local lattice distortions and aggregation of dimerons, associated with the JT-effect. This spin disordered phase is suppressed in the LSC compound owing to the decreasing number of JT-active ions. In the LSC compound the ratio of JT/non-JT ions is 2.49, which is close to the value 2.33 observed for $La_{0.7}Sr_{0.3}MnO_3$ compound for which there is also no GP-singularity.³⁵ However, the $La_{0.7}Sr_{0.3}MnO_3$ compound has a higher T_c (368.45 K), which can be explained by the reduction of the electronic bandwidth with Cu-substitution. Thus Cu-substitution plays two crucial roles, suppressing the disordered GP by reducing the number of JT-active ions and tuning the value of T_c towards room temperature by decreasing the electronic bandwidth. Apart from this, a reasonable value of the relative cooling power and isothermal entropy change near room temperature make B-site substitution with Cu-ions interesting for solid state cooling devices.

ACKNOWLEDGMENTS

The Swedish Foundation for Strategic Research (SSF, contract EM-16-0039) supporting research on materials for energy applications is gratefully acknowledged. Infrastructural grants by VR-RFI (#2017-00646_9) and SSF (contract RIF14-0053) supporting accelerator operation are gratefully acknowledged. Financial support by FITC HF RAS through project No. 45.22 (grant AAAA18-118012390045-2) is gratefully acknowledged. The authors are thankful to Sanchari Chakraborti for proofreading.

REFERENCES

- 1 A. Moreo, S. Yunoki, and E. Dagotto, Science (80-). **283**, 2034 (1999).
- 2 A.K. Pramanik and A. Banerjee, Phys. Rev. B - Condens. Matter Mater. Phys. **81**, 024431 (2010).
- 3 R.B. Griffiths, Phys. Rev. Lett. **23**, 17 (1969).
- 4 A.J. Bray, Phys. Rev. Lett. **59**, 586 (1987).
- 5 S. Banik and I. Das, J. Magn. Magn. Mater. **469**, 40 (2019).
- 6 T.L. Phan, P.S. Tola, N.T. Dang, J.S. Rhyee, W.H. Shon, and T.A. Ho, J. Magn. Magn. Mater. **441**, 290 (2017).
- 7 S.O. Manjunatha, A. Rao, P. Poornesh, W.J. Lin, and Y.K. Kuo, Phys. B Condens. Matter **498**, 82 (2016).
- 8 J. Deisenhofer, D. Braak, H.A. Krug Von Nidda, J. Hemberger, R.M. Eremina, V.A. Ivashin, A.M. Balbashov, G. Jug, A. Loidl, T. Kimura, and Y. Tokura, Phys. Rev. Lett. **95**, (2005).
- 9 X. Zheng, T. Gao, W. Jing, X. Wang, Y. Liu, B. Chen, H. Dong, Z. Chen, S. Cao, C. Cai, and V. V. Marchenkov, J. Magn. Magn. Mater. **491**, 165611 (2019).
- 10 W. Jiang, X. Zhou, and G. Williams, EPL (Europhysics Lett. **84**, 47009 (2008).
- 11 J. Khelifi, A. Tozri, F. Issaoui, E. Dhahri, and E.K. Hlil, Ceram. Int. **40**, 1641 (2014).
- 12 W. Jiang, X.Z. Zhou, G. Williams, Y. Mukovskii, and K. Glazyrin, Phys. Rev. B - Condens. Matter Mater. Phys. **77**, 064424 (2008).
- 13 J. Liu, W.-Q. Wang, H.-Y. Wu, T. Wang, Y. Tian, Feng-Ze Cao, and Ru Xing, J. Low Temp. Phys. **195**, 81 (2019).
- 14 J. Lyubina, J. Phys. D. Appl. Phys. **50**, 053002 (2017).
- 15 H.J. Whitlow, G. Possnert, and C.S. Petersson, Nucl. Inst. Methods Phys. Res. B **27**, 448 (1987).
- 16 J.P. Fryns, C. Parloir, J. Deroover, and H. Van den Berghe, Acta Paediatr. Belg. **31**, suppl V:33 (1993).
- 17 Y. Tokura and Y. Tomioka, J. Magn. Magn. Mater. **200**, 1 (1999).
- 18 R.D. Shannon, Acta Crystallogr. Sect. A **32**, 751 (1976).
- 19 L.B. McCusker, R.B. Von Dreele, D.E. Cox, D. Louë, and P. Scardi, J. Appl. Crystallogr. **32**, 36 (1999).
- 20 M.S. Kim, J.B. Yang, J. Medvedeva, W.B. Yelon, P.E. Parris, and W.J. James, J. Phys. Condens. Matter **20**, 255228 (2008).
- 21 M.A. Langell, C.W. Hutchings, G.A. Carson, and M.H. Nassir, J. Vac. Sci. Technol. A Vacuum, Surfaces, Film. **14**, 1656 (1996).
- 22 H.-S. Lee and H.-H. Park, Adv. Condens. Matter Phys. **2015**, 1 (2015).
- 23 T. Saitoh, A.E. Boquet, T. Mizokawa, H. Namatame, A. Fujimori, M. Abbate, Y. Takeda, and M. Takano, Phys. Rev. B **51**, 13942 (1995).
- 24 K. Ebata, H. Wadati, M. Takizawa, A. Fujimori, A. Chikamatsu, H. Kumigashira, M. Oshima, Y. Tomioka, and Y. Tokura, Phys. Rev. B - Condens. Matter Mater. Phys. **74**, 064419 (2006).
- 25 K. Arstila, J. Julin, M.I. Laitinen, J. Aalto, T. Konu, S. Kärkkäinen, S. Rahkonen, M. Raunio, J. Iktonen, J.-P. Santanen, T. Tuovinen, and T. Sajavaara, Nucl. Instruments Methods Phys. Res. Sect. B Beam Interact. with Mater. Atoms **331**, 34 (2014).
- 26 B.K. Banerjee, Phys. Lett. **12**, 16 (1964).
- 27 R. Skini, S. Ghorai, P. Ström, S. Ivanov, D. Primetzhofer, and P. Svedlindh, J. Alloys Compd. **827**, 154292 (2020).
- 28 R. Skini, M. Khelifi, and E.K. Hlil, RSC Adv. **6**, 34271 (2016).
- 29 R. Skini, A. Omri, M. Khelifi, E. Dhahri, and E.K. Hlil, J. Magn. Magn. Mater. **364**, 5 (2014).
- 30 P. Radaelli, G. Iannone, and M. Marezio, Phys. Rev. B - Condens. Matter Mater. Phys. **56**, 8265 (1997).
- 31 J. Yang, W.H. Song, Y.Q. Ma, R.L. Zhang, B.C. Zhao, Z.G. Sheng, G.H. Zheng, J.M. Dai, and Y.P. Sun, Phys. Rev. B - Condens. Matter Mater. Phys. **70**, 092504 (2004).
- 32 F. Bridges, L. Downward, J.J. Neumeier, and T.A. Tyson, Phys. Rev. B - Condens. Matter Mater. Phys. **81**, 184401 (2010).
- 33 P.S. Anil Kumar, P.A. Joy, and S.K. Date, J. Phys. Condens. Matter **10**, L269 (1998).
- 34 L. Downward, F. Bridges, S. Bushart, J.J. Neumeier, N. Dilley, and L. Zhou, Phys. Rev. Lett. **95**, 106401 (2005).
- 35 H. Zhang, L. Chen, Y. Li, H. Liu, Y. Chen, K. Chen, X. Dong, H. Yang, T. Gao, and Q. Li, in *J. Supercond. Nov. Magn.* (2011), pp. 1665-1672.